Bulletin of Engineering Geology and the Environment (2022) 81: 311
https://doi.org/10.1007/s10064-022-02804-x

ORIGINAL PAPER

The activity, segmentation, and evolution characteristics of large-scale landslides along the Anninghe active fault zone, Southwest China

Hongfu Zhou[1] · Fei Ye[2] · Wenxi Fu[2] · Yuting Wei[3] · Yadong Qin[1] · Wenqing Tang[1] · Tian Fang[1,4]

Received: 15 January 2022 / Accepted: 25 June 2022 / Published online: 14 July 2022

Abstract

The Anninghe fault zone located at the eastern margin of the Tibetan Plateau plays a significant role in affecting the evolution and distribution characteristics of geological disasters along the fault zone and in adjacent areas. In this paper, geological field surveys, remote sensing image interpretation, high-precision GPS monitoring, scanning electron microscopy (SEM) tests of fault gouges, and radon tests of fault zones were used to analyze the distribution characteristics, activity modes, and activity of the Anninghe fault zone. The Anninghe fault zone is divided into three sections, i.e., northern, middle, and southern sections. The middle section is further divided into three secondary sections. The results show that the present-day activity of the middle section is the strongest, followed by that of the northern section and then that of the southern section. Four types of fault-controlled modes of the large-scale landslides can be summarized, i.e., the landslide-entirety fault-controlled type (LEFT), landslide-crown fault-controlled type (LCFT), landslide-side fault-controlled type (LSFT), and landslide-toe fault-controlled type (LTFT). A strong positive correlation exists between the present-day activity of the Anninghe fault zone and the distribution density of large-scale landslides, and the more active a fault zone section is, the higher the density of large-scale landslides is.

Keywords Tibetan Plateau · Anninghe fault zone · Activity characteristics · Fault-controlled landslides · Fault-controlled sliding mode

Introduction

The Tibetan Plateau is slowly uplifting due to the northward subduction of the Indian plate to the Eurasian plate (Wang et al. 2008). Material on the eastern margin of the Tibetan Plateau rotates clockwise around the eastern Himalayan tectonic junction, and a series of large-scale active fault zones is distributed in the Tibetan Plateau and adjacent areas (He and Oguchi 2008). Most of the active faults are distributed along the eastern margin of the Tibetan Plateau (Tang et al. 2016), and these faults are characterized by the most frequent seismic activity, the most complex geological environment, and a high incidence of geological disasters (Wen et al. 2008; Qu et al. 2018; Ye et al. 2021). Recently, the eastern margin of the Tibetan Plateau has been of great concern to the local government, scholars, and engineers in regard to the planning and construction of the Sichuan-Tibet railway and Sichuan-Tibet expressway (Wu et al. 2020; Chen et al. 2020).

The Anninghe fault is located on the southeastern margin of the Tibetan Plateau (Fig. 1). It is an important active fault along the eastern margin of the Tibetan Plateau (Ran et al. 2008; Ren et al. 2010; Ren (2014) and is also an earthquake-generating fault zone of Southwest China (He and Ikeda 2007). Many destructive earthquakes have occurred along this fault zone, denoting high activity (Wang et al. 2014, 2017). However, cities and towns are distributed along the Anninghe fault zone. In addition, numerous key projects have been planned, are under construction, or have been completed, including the G5 Beijing-Kunming expressway, Chengdu-Kunming railway,

✉ Hongfu Zhou
zhf800726@163.com

1 Chengdu Center, China Geological Survey, Chengdu, China

2 State Key Laboratory of Hydraulics and Mountain Rivers Protection, Sichuan University, Chengdu, China

3 Sichuan Institute of Geological Engineering Investigation Group Co. Ltd, Chengdu, China

4 College of Earth Science and Engineering, Shandong University of Science and Technology, Qingdao, China

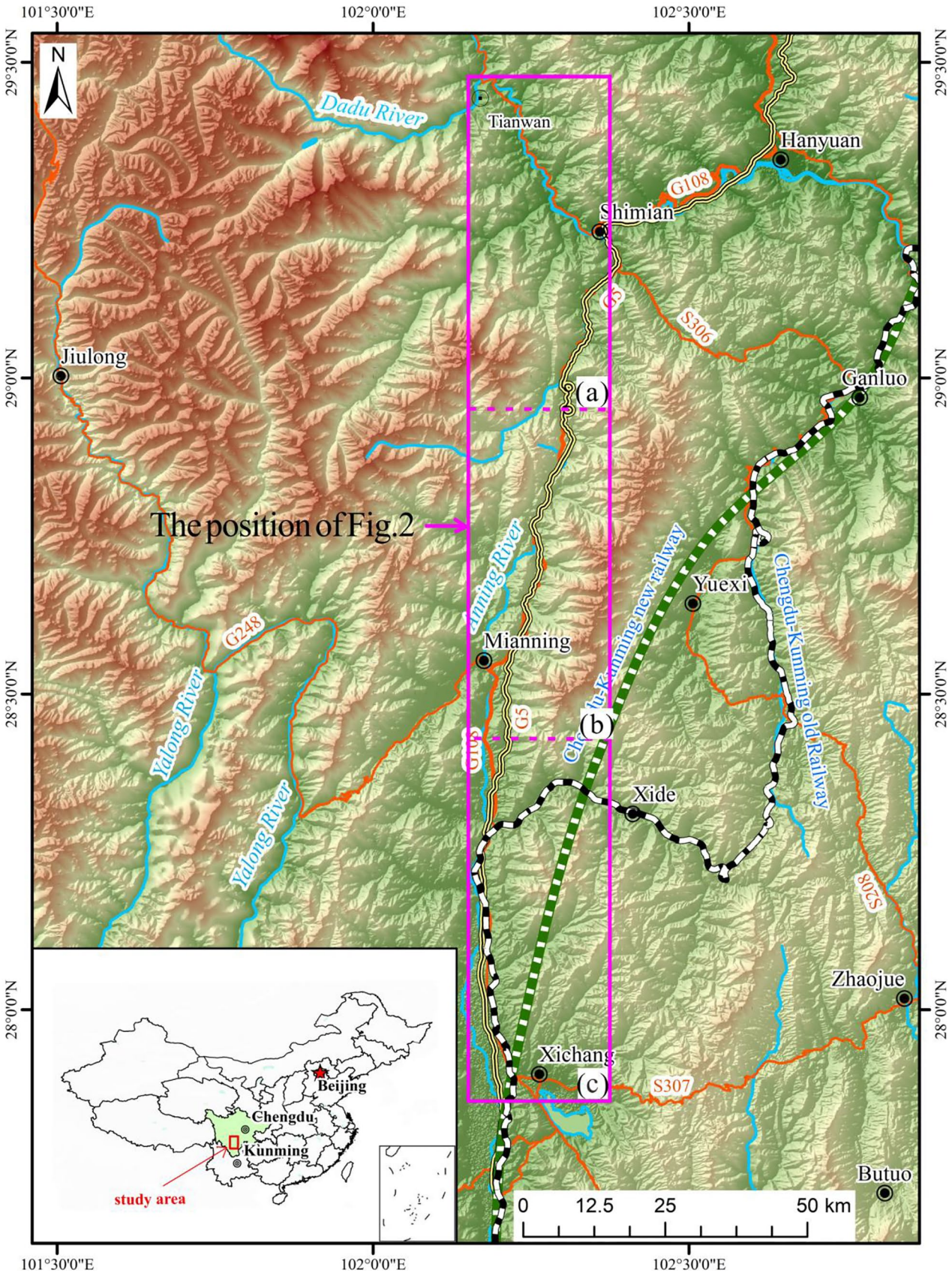

Fig. 1 Location of the study area and main infrastructures in this area

Xichang satellite launch center, and Xichang Qingshan airport. The geological conditions of the Anninghe fault zone have been the research focus of numerous engineering and seismic geologists (Cheng et al. 2021).

Generally, a large-scale fault zone consists of some secondary faults of different stages, properties, and scales. The activity of a fault exhibits notable heterogeneity across time, space, and intensity throughout the long-term geological evolution process (Li et al. 1998). The geometric structure, activity time, activity mode, moving velocity, and seismic activity of a fault zone also vary (Ahmad 2021). The Anninghe fault zone is a representative reflection of the nonuniformity of segmental activity (Yi et al. 2004).

Fault zones play a key role in influencing and controlling the evolution and distribution of landslides (Osmundsen et al. 2009). On the one hand, fault zones can destroy the rock mass structure and integrity of a slope. Loose soil or rock slopes are prone to fail under rainfall, and a higher distribution density of landslides is recorded on both sides of fault zones (Scheingross et al. 2013). On the other hand, the sudden movements of fault zones (earthquakes) can trigger numerous types of coseismic landslides and secondary disasters (Xu et al. 2020), leading to numerous casualties and significant property losses (Ho et al. 2020; Zhao et al. 2021). In addition, geological structure, especially that of fault zones, also plays a key role in controlling the stability of landslides (Stead and Wolter 2015; Vick et al. 2020). Unfortunately, few studies have been conducted on the present-day activity of fault zones or on the relationship between active segmentation and the distribution of large-scale landslides along the Anninghe fault zone, as most researchers have focused on surface rupture characteristics, historical activity, and earthquake prediction and evaluation (He and Oguchi 2008; Ran et al. 2008; Ren 2014).

A 5-year engineering geological investigation and study of the Anninghe fault zone was carried out and involved data collection, geological surveys, remote sensing image interpretation, high-precision GPS monitoring, scanning electron microscopy (SEM) tests of the fault gouge, and radon tests of the fault zone. The spatial distribution characteristics, historical earthquakes, activity modes, and activity of the Anninghe fault zone were found to be notable. The present-day activity characteristics of different sections of the Anninghe fault zone are thoroughly considered in this paper. According to the evolution and distribution of large-scale landslides, fault-control sliding modes are summarized, and the relationship between the active section and evolution characteristics of large-scale landslides along the Anninghe fault zone is analyzed. The presented results are of great significance to the planning and construction of large-scale infrastructures and disaster prevention and mitigation in Southwest China.

Geological setting

The Anninghe fault zone is located in southwestern China at the intersection of the southeastern margin of the Tibetan Plateau and the Yunnan-Guizhou Plateau. The zone is an important part of the Y-shaped fault system in China. The Anninghe fault zone is characterized by long-term activity, multiple activities, high-intensity activity, and a high sliding rate. The activity time of the Anninghe fault zone runs from the Mid-Late Pleistocene to the Holocene. According to geological surveys and remote sensing interpretations, the authors further subdivided the Anninghe fault zone into 17 secondary faults of different sizes, shapes, and properties (Table 1).

The Anninghe fault zone originates in the town of Tianwan, Shimian County, in the north; connects to the southern end of the Xianshuihe fault; and divides into two nearly parallel north–south strike faults after passing through the towns of Xieluo, Zimakua, Yihai, and Xiaoyanjing. The fault zone is a single fault zone consisting of a series of secondary faults north of the town of Xiaoyanjing, while two parallel oblique fault zones consist of a series of secondary faults south of the town of Xiaoyanjing (Fig. 2), i.e., an east branch fault distributed from Xiaoyanjing and Houshan to Luji and a west branch fault distribution from Xiaoyanjing, Linli, Lugu, Yuehua, and Lizhou to Xichang.

Active characteristics of the Anninghe fault zone

Activity mode of the Anninghe fault zone

The mode of fault activity is an important component of engineering geological surveys of fault zones, and it is also an important reference measure for dividing potential seismic areas. Faults can be divided into creep slip faults and stick slip faults based on the nature of activity. Generally, moderate to minor earthquakes are induced by creep slip faults due to long-term, relatively slow displacement acting as an inhibitory factor of strain energy accumulation. By contrast, the dislocation displacement of a stick slip fault occurs suddenly, usually triggering destructive earthquakes. Therefore, studying the mode of fault activity is not only helpful for predicting the range of fault-induced earthquakes but also advantageous for analyzing the genetic mechanism and distribution characteristics of geological disasters along faults.

Research results have shown that the stress microshape characteristics of quartz particles in fault gouges can reflect the mode of fault activity (Zhang et al. 1994, 2002;

Table 1 Development characteristics of secondary faults of the Anninghe active fault zone

No	Name	Length/km	Strike/°	Dip direction/°	Dip/°	Property
F1	Zimakua fault	30	N10 ~ 20°E	NW	60–80	Sinistral strike slip (with thrust)
F2	Paisigedi fault	22	NNE	W	60–80	Sinistral strike slip (with thrust)
F3	Yejidong fault	4	N20 ~ 30°E	NW	60	Sinistral strike slip (with thrust)
F4	Yihai fault	12	N10°E	W&E	70–80	Sinistral strike slip (with thrust)
F5	Mixiluogou fault	11	NNE	W	60	Sinistral strike slip (with thrust)
F6	Shawan fault	8	S ~ N	W&E	35–75	Sinistral strike slip (with thrust)
F7	Linlicun fault	6	N10 ~ 25°E	SE	62	Sinistral strike slip (with thrust)
F8	Shilong fault	7	NNW	NEE	40–80	Sinistral strike slip (with thrust)
F9	Shaguoshu fault	4	S ~ N	E	75	Sinistral strike slip (with thrust)
F10	Lugu fault	12	N20°E	NW	60–80	Sinistral strike slip (with thrust)
F11	Yijiahaizi fault	1.5	N10°W	SW	70	Sinistral strike slip
F12	Yangfushan fault	8	S ~ N	W&E	65–75	Sinistral strike slip (with thrust)
F13	Shejinuo fault	2.5	S ~ N	E	80	Sinistral strike slip (with thrust)
F14	Hongshanzui fault	14	N10 ~ 20°W	NE	60	Sinistral strike slip (with thrust)
F15	Shayema fault	31.5	S ~ N	W	73	Sinistral strike slip (with thrust)
			N10°E	SE	50	Sinistral strike slip (with thrust)
F16	Dapingzi fault	23	N10°W	NE	50–75	Sinistral strike slip (with thrust)
F17	Luji fault	6	S ~ N	E	65–70	Sinistral strike slip (with thrust)

Kanaori et al. 1985), and this characteristic reflects the process of fault activity and its dynamic characteristics. The stress microshape represents the stick slip movements of a fault, including wedge pit, conchoidal fracture, river pattern, wallner line, dense cleavage, triangular pit, linear slickensides, and linear microfault. Their edges and peaks have sharp apices though a little blunt at each end (Fig. 4b, c, h), and they are characterized by simple and smooth faces (Fig. 4a, g). Sometimes, minute cracks can be observed at the surface with the length of 50 to 100 um (Fig. 4d). Moreover, some stress microshapes have well-defined round shapes with considerably undulated surfaces (Fig. 4e). By contrast, fatigue striations, arc slickensides, tension fractures, spoon-shaped grinding pits, spoon-shaped slickensides, and orange peel-shaped spherulites denote a predominantly creep slip fracture. The surfaces of quartz particles of creep slip type are generally smooth, though slightly undulated (Fig. 3d, e), or approximate rounded (Fig. 3f). The quartz particles are characterized by small angular shapes (Fig. 3a) and nearly smooth surfaces with small undulations (Fig. 3b) or irregular small holes of 20 to 100 um in length (Fig. 3c). In addition, cleavage steps, oval pits, and irregular pits are regarded as transition types (Kanaori et al. 1980).

According to the above results, 21 fault gouge samples were taken from the seventeen Anninghe secondary faults, and the sampling locations are shown in Fig. 2. The stress microshape characteristics of quartz particles in the fault gouge were observed under a Hitachi S-4800 scanning electron microscope (SEM). To ensure that the observed suspicious particles were quartz particles, the particles were analyzed by energy spectroscopy (Figs. 3 and 4). Modes of fault activity were distinguished as follows:

A microshape is mainly characterized by stick slip movement with less creep slip, denoting a stick slip fault gouge.
A microshape is mainly characterized by creep slip movement with less stick slip, denoting a creep slip fault gouge.
The presence of both stick and creep slip characteristics with more of the latter denotes a creep-stick slip fault gouge. When there are more stick slip characteristics, this denotes a stick-creep slip fault gouge.

According to the test results for the stress microshape characteristics of quartz particles in the fault gouge, the activity modes of the 17 secondary faults of the Anninghe fault zone were obtained by combining the classification and frequency distribution of the SEM corrosion structure on the quartz surface of the fault gouge (Xu et al. 1987) (Table 2). The F1 fault in the northern section of the Anninghe fault is mainly a creep slip fault with an active age of the Mid-Late Pleistocene to the Holocene and strong activity in the Mid-Late Pleistocene. The activity modes of the F2 to F17 faults are mainly stick slip modes, while the F3, F4, F7, F9, F13, F14, F16, and F17 faults also have creep slip characteristics. In addition, the activity mode of No. 16 (southern section of F14) is stick-creep slip, dominated by creep slip. The activity

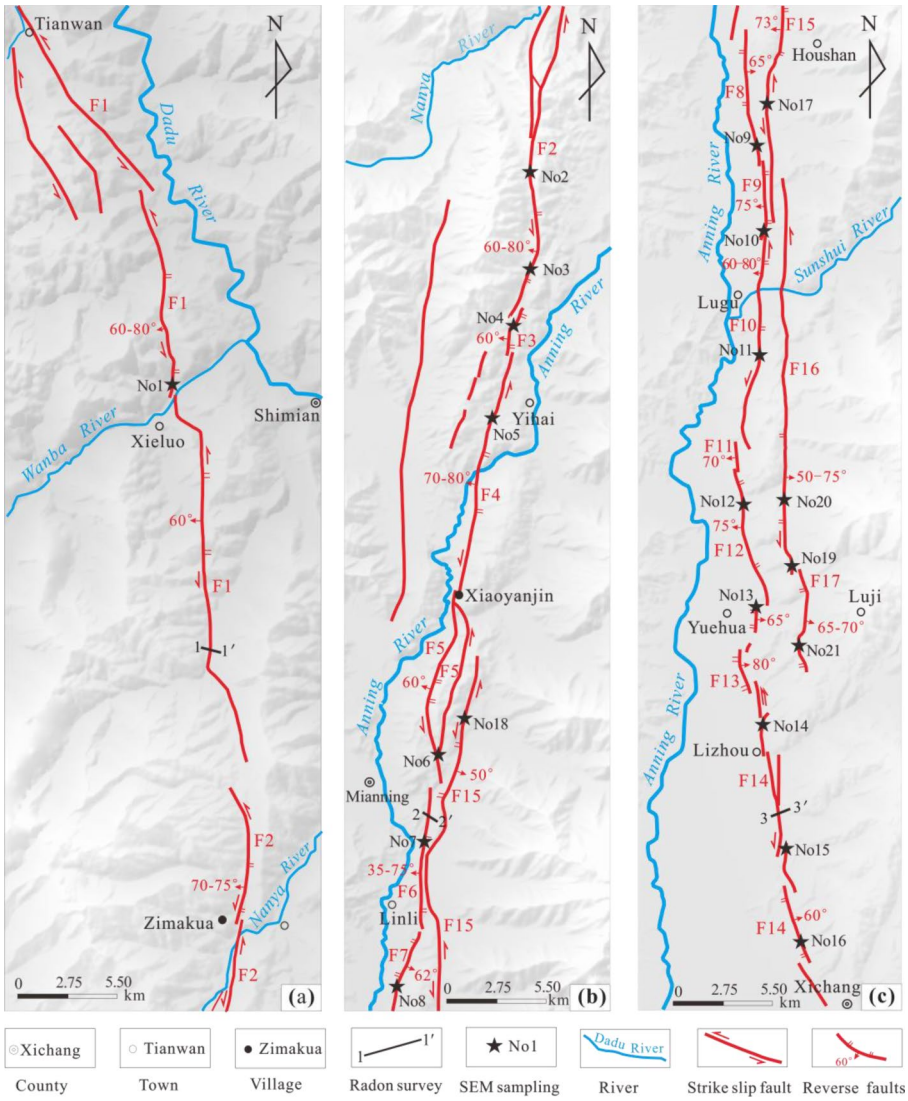

Fig. 2 Planar distribution of secondary faults in the Anninghe active fault zone: **a** the northern section, **b** the middle section, and **c** the southern section. F1, Zimakua fault; F2, Paisigedi fault; F3, Yejidong fault; F4, Yihai fault; F5, Mixiluogou fault; F6, Shawan fault; F7, Linlicun fault; F8, Shilong fault; F9, Shaguoshu fault; F10, Lugu fault; F11, Yijiahaizi fault; F12, Yangfushan fault; F13, Shejinuo fault; F14, Hongshanzui fault; F15, Shayema fault; F16, Dapingzi fault; F17, Luji fault

F1: Zimakua fault; F2: Paisigedi fault; F3: Yejidong fault; F4: Yihai fault; F5: Mixiluogou fault; F6: Shawan fault; F7: Linlicun fault; F8: Shilong fault; F9: Shaguoshu fault; F10: Lugu fault; F11: Yijiahaizi fault; F12: Yangfushan fault; F13: Shejinuo fault; F14: Hongshanzui fault; F15: Shayema fault; F16: Dapingzi fault; F17: Luji fault

modes of the eastern and western branches of the Anninghe fault differ slightly from those of the Xiaoyanjing to Luji sections. Among all 17 secondary faults, the F2, F3, F5, F8, F10, and F16 were the most active during Late Pleistocene age; the F9, F12, and F15 were the most active during the Holocene age; the F1, F4, F6, and F7 were the most active during the Mid and Late Pleistocene age; the F14 was the most active during the Early and Middle Pleistocene age; and the F13 was the most active during the Early Pleistocene age. The faults with strong activity during the Holocene age are mainly of the stick slip activity mode, e.g., the F9, F10, F11, F12, and F15 faults. However, the activities of the F6, F7, F8, F16, and F17 faults are weak during the Holocene age, and the faults are of the stick-creep slip activity mode. The F13 and F14 faults in the southern section of the Anninghe fault are mainly of the stick slip activity mode and exhibit the creep slip activity mode with strong activity in the Early-Middle Pleistocene in some sections.

Activity of the Anninghe fault zone

Radon, a radioactive gas, has stable chemical properties and strong migration ability. It can continuously migrate and release into the Earth's surface along the fracture

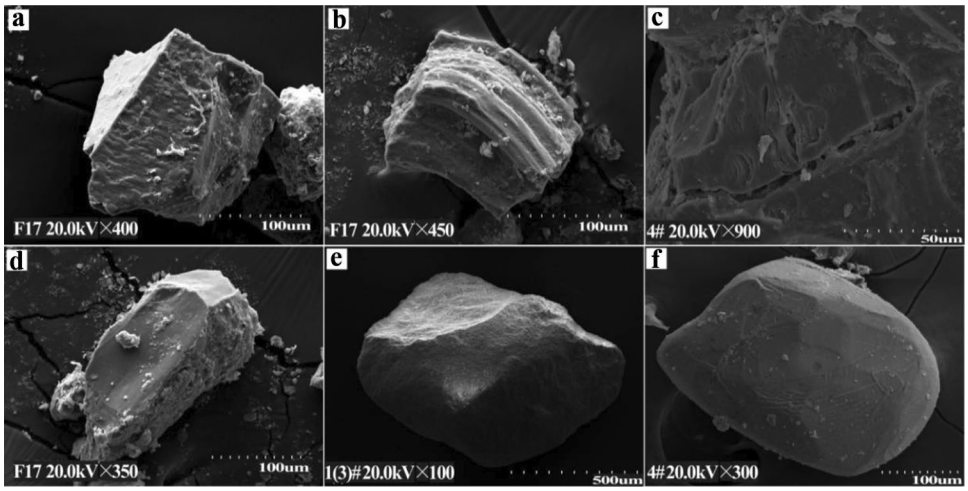

Fig. 3 Surface micromorphology of quartz debris in the fault gouge of the Anninghe active fault (creep slip). **a** Fatigue striations; **b** arc slickensides; **c** tension fracture; **d** spoon-shaped grinding pit; **e** spoon-shaped slickensides; **f** orange peel-shaped spherulite

zone of a fault and its vicinity. Radon is often used as an indicator element of deep information below the Earth's surface. Research results show abnormally high levels of radon along active faults (Yang et al. 2018). Consequently, the spatial locations of faults below the surface can be detected, and the activity of faults can be evaluated by conducting radon tests. In this paper, three radon test profiles are deployed on the Zimakua fault (F1), Shawan fault (F6), and Hongshanzui fault (F14). The profile locations are shown in Fig. 2, and the corresponding test results are shown in Fig. 5.

The average radon concentration of the Zimakua fault (F1) profile is 2869 Bq/m^3, while the average radon concentration is 4137 Bq/m^3 near the fault fracture, which is 1.44 times that of the whole profile. The maximal radon concentration of the fault fracture is 7211.9 Bq/m^3, which is 2.51 times that of the whole profile.

The Shawan fault (F6) is located in a landslide area, which may have a negative influence on the test results. The average radon concentration is 3222 Bq/m^3 along the profile, and the maximal radon concentration is 9016.7 Bq/m^3 near the fault fracture, which is 2.80 times that of the whole profile.

The average radon concentration of the profile of the Hongshanzui fault (F14) is 4598 Bq/m^3 and the average radon concentration is 7964 Bq/m^3 near the fault fracture,

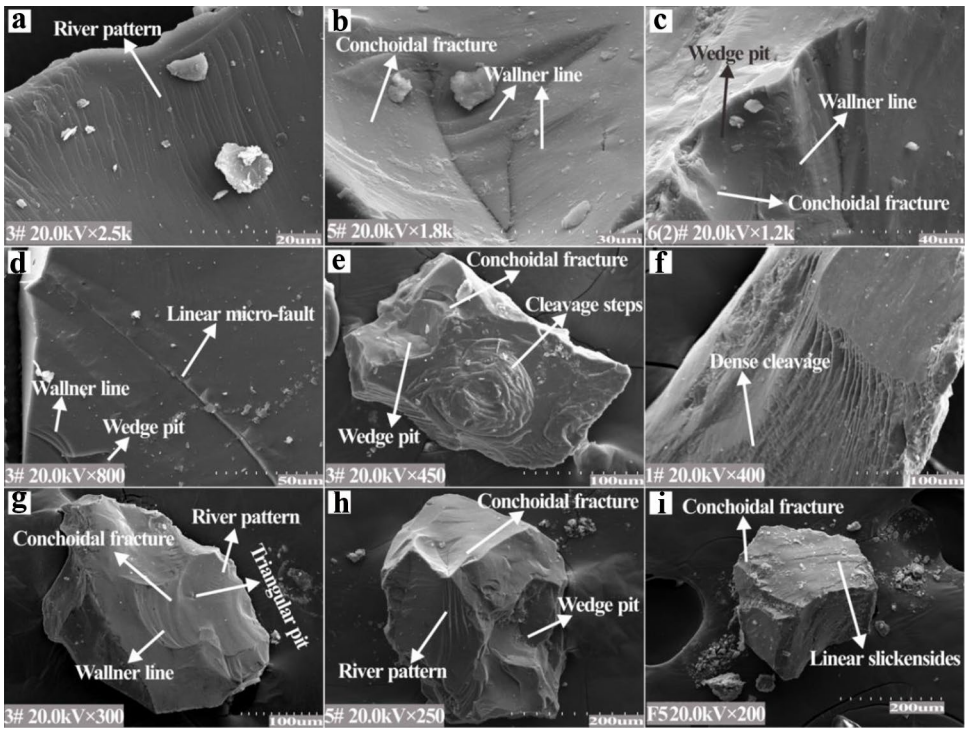

Fig. 4 Surface micromorphology of quartz debris in the fault gouge of the Anninghe active fault (stick slip). **a** River pattern; **b** Conchoidal fracture, Wallner line; **c** Wedge pit, Wallner line, Conchoidal fractrure; **d** Linear micro-fault, Wallner line, Wedge pit; **e** Conchoidal fracture, Cleavage steps, Wedge pit; **f** Dense cleavage; **g** Conchoidal fracture, River pattern, Triangular pit, Wallner line; **h** Conchoidal fracture, Wedge pit, River pattern; **i** Conchoidal fracture, Linear slickensides

Table 2 Age and nature of secondary fault activity identified by SEM testing of the fault gouge of the Anninghe fault zone

Sample	Fault	Age of fault activity (from strong to weak)	Microshape of faults	Nature of faults activity
No. 1	F1	Mid-Late Pleistocene; Holocene	Spoon-shaped slickensides; arc slickensides; orange peel-shaped spherulite; cleavage steps; oval pit	Creep slip
No. 2	F2	Late Pleistocene; Holocene; Middle Pleistocene	Conchoidal fracture; triangular pit; linear slickensides; arc slickensides; spoon-shaped slickensides; orange peel-shaped spherulite	Stick-creep slip, dominated by stick slip
No. 3	F2	Late Pleistocene-Holocene; Middle Pleistocene	Conchoidal fracture; river pattern; radial fracture; triangular pit; linear slickensides	Stick slip
No. 4	F3	Late Pleistocene; Holocene; Early Middle Pleistocene	Conchoidal fracture; river pattern; radial fracture; triangular pit; linear slickensides; oval pit; tension fracture	Stick-creep slip, dominated by stick slip
No. 5	F4	Mid-Late Pleistocene; Early Pleistocene; Holocene	Conchoidal fracture; triangular pit; linear slickensides; arc slickensides; spoon-shaped slickensides; fatigue striations; circular spherulite	Stick-creep slip, dominated by stick slip
No. 6	F5	Late Pleistocene; Middle Pleistocene; Holocene	Triangular pit; conchoidal fracture; radial fracture; linear slickensides	Stick slip
No. 7	F6	Mid-Late Pleistocene; Early Pleistocene; Holocene	Conchoidal fracture; triangular pit; circular spherulite	Stick-creep slip
No. 8	F7	Mid-Late Pleistocene; Early Pleistocene; Holocene	Triangular pit; conchoidal fracture; radial fracture; river pattern; fatigue striations; circular pit; spoon-shaped slickensides	Stick-creep slip, dominated by stick slip
No. 9	F8	Late Pleistocene; Holocene; Middle Pleistocene	Conchoidal fracture; triangular pit; wedge pit; circular spherulite	Stick-creep slip
No. 10	F9	Holocene; Late Pleistocene	Triangular pit; conchoidal fracture; radial fracture; linear slickensides; fatigue striations; circular spherulite; tension fracture	Stick-creep slip, dominated by stick slip
No. 11	F10	Late Pleistocene-Holocene; Middle Pleistocene	Triangular pit; conchoidal fracture; wedge pit; river pattern; linear slickensides; circular spherulite	Stick slip
No. 12	F12	Holocene; Late Pleistocene; Early-Middle Pleistocene; Pliocene	Triangular pit; conchoidal fracture; radial fracture; river pattern; linear slickensides; oval pit	Stick slip
No. 13	F13	Early Pleistocene; Early-Middle Pleistocene; Pliocene; Late Pleistocene-Holocene	Conchoidal fracture; cleavage steps; tension fracture; fatigue striations	Stick-creep slip, dominated by stick slip
No. 14	F14	Late Pleistocene; Holocene; Middle Pleistocene	Conchoidal fracture; triangular pit; river pattern; wedge pit; linear slickensides	Stick slip
No. 15	F14	Early-Middle Pleistocene; Pliocene to Holocene	Linear slickensides; irregular pit; circular spherulite; linear slickensides	Stick slip
No. 16	F14	Early-Middle Pleistocene; Late Pliocene; Holocene	Fatigue striations; circular spherulite; arc slickensides; conchoidal fracture	Stick-creep slip, dominated by creep slip
No. 17	F15	Holocene; Late Pleistocene; Middle Pleistocene	Conchoidal fracture; triangular pit; wedge pit; linear slickensides; cleavage steps	Stick slip
No. 18	F15	Holocene; Late Pleistocene; Middle Pleistocene	Conchoidal fracture; triangular pit; river pattern; wedge pit; linear slickensides	Stick slip
No. 19	F16	Late Pleistocene; Holocene; Pliocene-Early Pleistocene	Conchoidal fracture; river pattern; triangular pit; linear slickensides; fatigue striations; irregular pit; arc slickensides	Stick-creep slip
No. 20	F16	Late Pleistocene; Holocene; Middle Pleistocene; Pliocene-Early Pleistocene	Conchoidal fracture; triangular pit; cleavage steps; irregular pit; tension fracture; fatigue striations	Stick-creep slip, dominated by stick slip
No. 21	F17	Late-Early Pleistocene; Late Pleistocene; Holocene; Pliocene	Conchoidal fracture; triangular pit; linear slickensides; cleavage steps; radial fracture	Stick-creep slip, dominated by stick slip

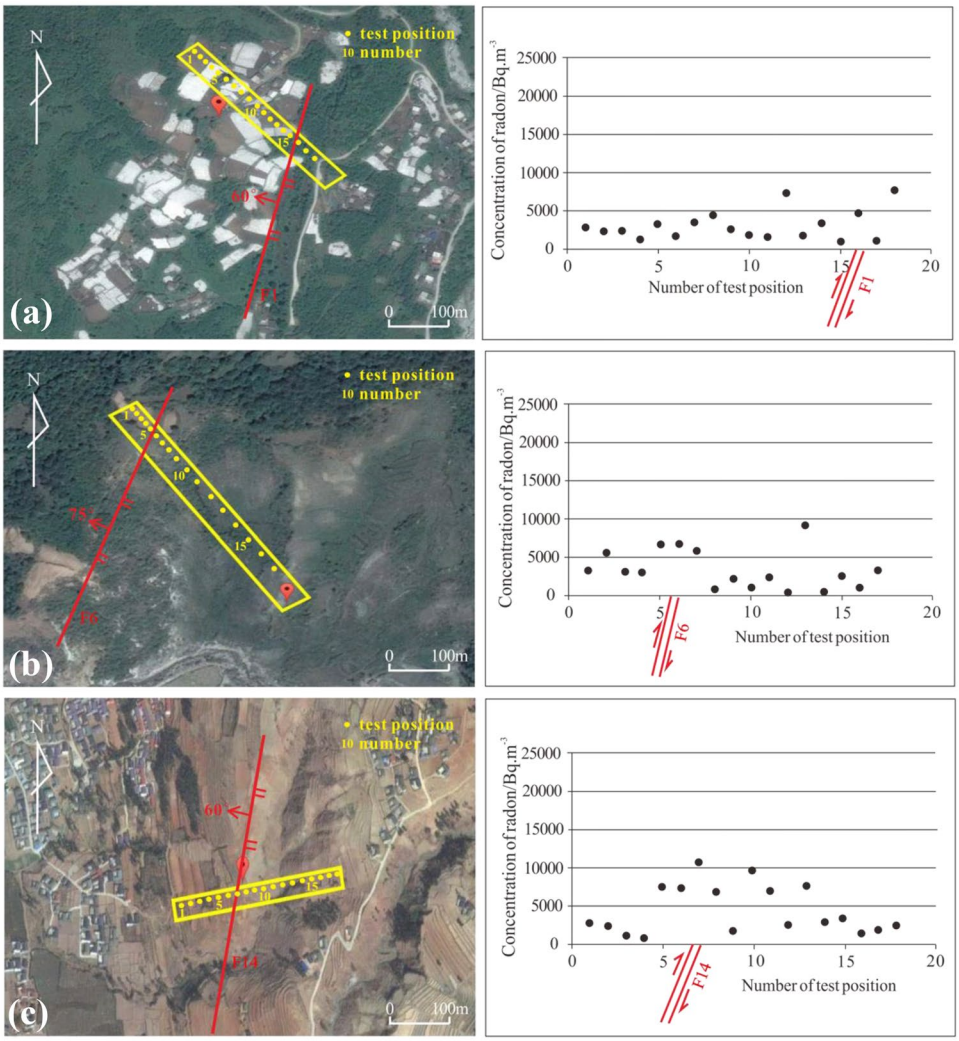

Fig. 5 Radon test location and results of secondary faults of the Anninghe active fault zone, **a** radon test result of F1, 1–1′ profile of Fig. 2; **b** radon test result of F6, 2–2′ profile of Fig. 2; **c** radon test result of F14, 3–3′ profile of Fig. 2

which is 1.73 times that of along the profile. The maximal radon concentration is 10629.2 Bq/m^3 near the fault fracture, which is 2.3 times that of the whole profile.

The maximum radon concentration near the fault fracture is 2.3–2.8 times the average value along the fault profile. These test results indicate that the Anninghe fault zone is an active fault, and the activity of the middle section is stronger than that of the northern section.

Historical earthquakes along the Anninghe fault zone

The number and magnitude of historical earthquakes along a fault and its adjacent areas are important indices for evaluating fault activity. According to the National Earthquake Data Center (https://data.earthquake.cn/), relevant county annals, and literature, the timing, epicenter location, magnitude, and epicenter intensity of destructive earthquakes with magnitudes of greater than Ms 4.7 along the Anninghe fault zone and its vicinity are shown in Fig. 6 and Table 3.

According to the epicenter location, frequency, and intensity of historical earthquakes, the Anninghe fault zone has a significant controlling effect on seismic activity in the study area. Most of the earthquake epicenters are located along the Anninghe fault zone. A total of 31 destructive earthquakes (Ms ≥ 4.7) have occurred in the study area, including 7 earthquakes with magnitudes of Ms 4.7 ~ 4.9, 11 with magnitudes of Ms 5.0 ~ 5.9, 11 with magnitudes of Ms 6.0 ~ 6.9, and 2 with magnitudes of Ms 7.5, for which the epicenter intensity was X degrees and the epicenters were located at the cities of Lizhou and Tianba, Xichang.

Many historical earthquakes are distributed along the Tianwan-Zimakua section, and the number of earthquakes occurring accounts for more than 70% of those of the whole Anninghe fault zone (Xu 1988); however, only one fault (F1) is located in this area. In addition, the magnitudes of these earthquakes were less than Ms 5.0 and mainly recorded Ms values of 2.0 ~ 4.0. This phenomenon is mainly determined by the creep slip nature of a fault.

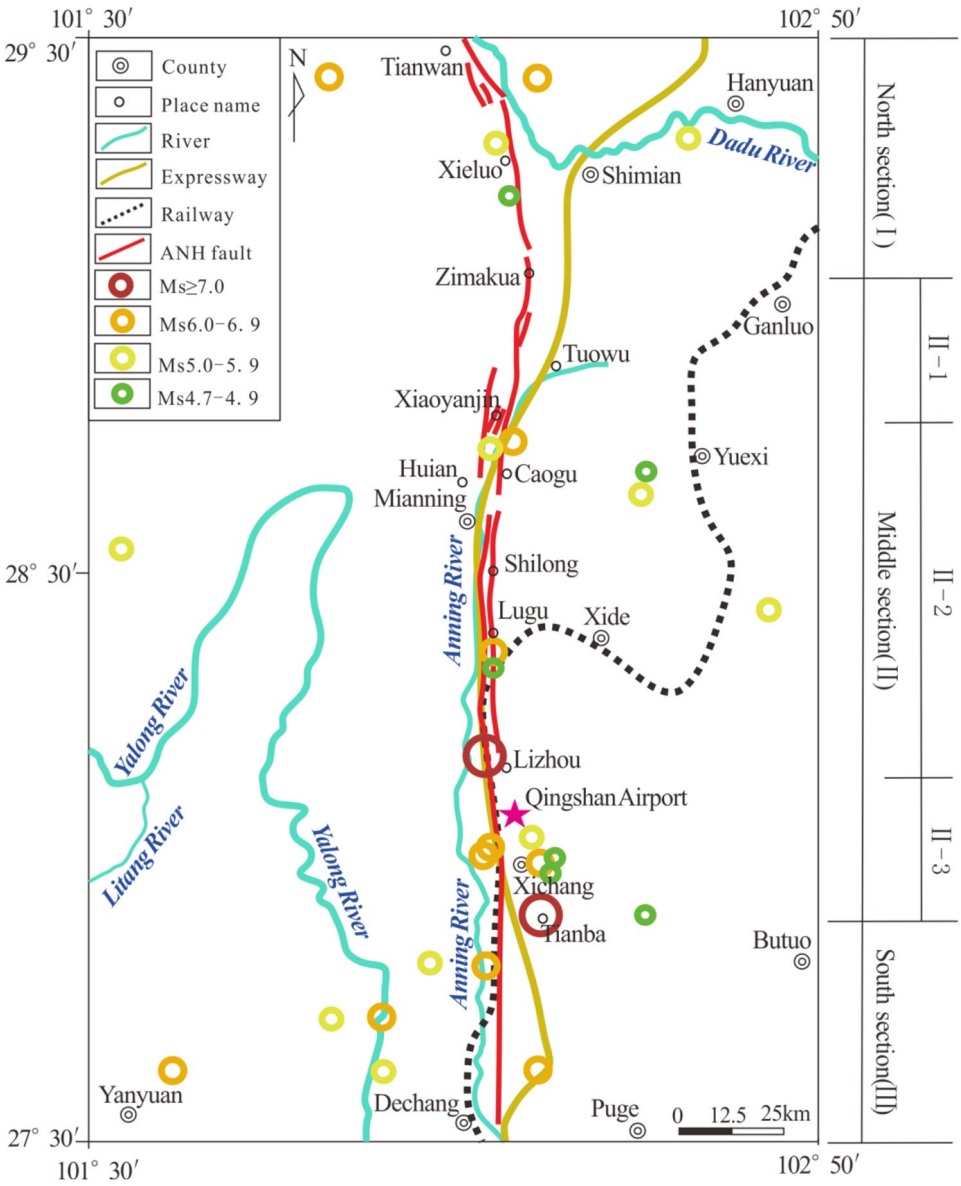

Fig. 6 Epicenter location of Ms ≥ 4.7 earthquakes and section along the Anninghe fault zone

Many historical earthquakes (Ms ≥ 6.0) have been distributed along the Zimakua-Lizhou section of the Anninghe fault zone; e.g., the Xiaoyanjing Ms 6.0 earthquake occurred on August 19, 1913, and the Shilong Ms 6.75 earthquake occurred on September 30, 1952. This section includes the F2 ~ F12, F16, and F17 faults. Such phenomena are related to the stick-creep slip activity mode of the faults.

Some historical earthquakes of high magnitudes occurred along the Lizhou-Xichang section. This section is the most active of the whole Anninghe fault zone, including the F13 and F14 faults. Two strong earthquakes (Ms 7.5) that occurred on March 29, 1536, and September 12, 1850, were distributed in this section. This is the case because the fault belongs to the stick slip activity mode, and the section is located at the intersection of the Anninghe and Zemuhe faults. There have been few historical earthquakes of low magnitudes in the southern Xichang area, denoting weak fault activity.

Segment characteristics of the Anninghe fault zone

The Anninghe fault zone is a complex fault zone consisting of 17 secondary faults. The activity characteristics of the Anninghe fault are segmented due to differences in spatial distribution characteristics, activity modes, and tectonic stress environments of the secondary faults. In this study, the Anninghe fault zone is divided into three sections (northern, middle, and southern sections) with different activity characteristics on the basis of spatial geometrical shapes, structures, activity modes, and active intensity and historical seismic activity levels (Fig. 6, Table 4).

Table 3 Characteristics of Ms ≥ 4.7 earthquakes along the Anninghe fault zone and its vicinity (N: 27°30′ ~ 29°30′; E: 101°30′ ~ 102°50′)

Occurrence time	Epicenter		Magnitude/Ms	Epicenter intensity	Epicenter site
Year. Month. Date	Latitude/°	Longitude/°			
B.C116	27.5	102.3	6.0 ~ 7.0	≥VIII	Gucheng village, Xichang City
624.08.15	27.9	102.2	6.7	IX	Xiaomiao Town, Xichang City
814.04.06	27.9	102.2	6.5	VIII	Xiaomiao Town, Xichang City
1427.00.00	27.9	102.3	5.0	VII	Zhangjiaao, Xichang City
1467.01.19	27.6	102.0	6.5	VIII	Jinhe Town, Yanyuan County
1478.08.17	27.5	101.6	6.0	VII	Huoyakou, Yanyuan County
1480.09.22	28.6	102.5	5.5	VII	Dingshan Town, Yuexi County
1489.01.06	27.9	102.2	6.75	IX	Xiaomiao Town, Xichang City
1495.02.10	27.9	102.3	4.7	/	Zhangjiaao, Xichang City
1499.04.02	27.9	102.3	4.7	/	Zhangjiaao, Xichang City
1536.03.29	28.1	102.2	7.5	X	Lizhou Town, Xichang City
1732.01.29	27.7	102.2	6.75	IX	Youjun Town, Xichang City
1830.07.00	27.8	102.5	4.7	/	Hatujuemo, Xichang City
1850.09.12	27.8	102.3	7.5	X	Tianba, Xichang City
1881.06.00	28.6	102.5	4.75	VI	Dingshan Town, Yuexi County
1913.8.19	28.7	102.25	6.0	VIII	Xiaoyanjin, Mianning County
1923.08.00	28.7	102.2	5.5	VII	Daqiao Town, Mianning County
1935.04.28	29.4	102.3	6.0	/	Chashan, Shimian County
1944.08.03	28.5	101.5	5.75	/	Maliuwan, Jiulong County
1951.03.16	29.3	102.6	5.0	VI	Xinmin Town, Shimian County
1951.05.10	27.5	102.0	5.5	VII	Fujiawan, Dechang County
1952.02.06	27.9	102.3	5.0	VI	Gaojian Town, Xichang City
1952.09.30	28.3	102.2	6.75	IX	Shilong Town, Mianning County
1962.02.27	27.6	101.9	5.5	VII	Yousuo Town, Yanyuan County
1972.05.07	27.95	102.3	4.7	VI	Tianba, Xichang City
1975.01.15	29.4	101.9	6.2	VIII	Liuba Town, Kangding City
1977.01.13	28.27	102.2	4.8	VI	Lugu Town, Mianning County
1989.06.09	29.27	102.22	5.2	VII	Anshun Town, Shimian County
2008.06.18	29.17	102.25	4.7	VI	Jizipin Town, Shimian County
2014.10.01	28.38	102.74	5.0	VI	Baoshi Town, Yuexi County
2018.10.31	27.70	102.08	5.1	VI	Mopan Town, Xichang City

1. ***Northern section (I): from Tianwan to Zimakua***

   This area is approximately 50 km long, only includes the Zimakua fault (F1), and has a simple structure. The section is a single fault zone composed of multiple secondary small faults, and the head and tail of the small faults are not connected to each other. The activity and movement speed of the fault are moderate, and the structure is moderately complex in this section. As the fault belongs to the creep slip activity mode, only small- and moderate-magnitude earthquakes (> Ms 7.0) have occurred in this section.

Table 4 Displacement rates (2008–2016) and fault properties of the Anninghe fault

Faults segment		Location	Displacement rate (mm/a)	Earthquake activity	Sliding mode
North section	I	Tianwan to Zimakua	1.66 ± 0.52	Quantity was large, strength was weak	Creep slip
Middle section	II-1	Zimakua to Xiaoyanjin	1.20 ± 0.38	Quantity was small, strength was moderate	Stick-creep slip
	II-2	Xiaoyanjin to Lizhou	2.98 ± 1.73	Quantity was large, strength was strong	Stick slip
	II-3	Lizhou to Xichang	8.15 ± 1.31	Quantity was large, strength was strong	Stick slip
South section	III	South of Xichang	0.96 ± 0.74	Quantity was small, strength was weak	Creep slip

Displacement rate data are obtained from Tang et al. (2016)

2. ***Middle section (II): from Zimakua to the city of Xichang***

   This fault is very complex in structure with strong activity and a high movement speed. Historical strong earthquakes have mainly occurred in this section due to the stick slip nature of the fault. According to the geometric shape, activity mode, and active intensity of the fault zone, the middle section of the Anninghe fault zone is further divided into three subsections, i.e., the Mid-North section, Mid-Middle, and Mid-South sections. Mid-North section (II-1): from Zimakua to Xiaoyanjin This area is approximately 40 km long and has a simple plane structure. This section includes the Paisgedi fault (F2), Yejidong fault (F3), and Yihai fault (F4). Generally, the fault movement speed is relatively low and of the stick-creep slip activity mode. Earthquake intensity levels are of moderate magnitude in this section. Mid-Middle section (II-2): from Xiaoyanjin to Lizhou This area is approximately 55 km long and composed of two nearly parallel secondary fault zones. The eastern fault includes 8 faults, i.e., the Mixiluogou fault (F5), Shawan fault (F6), Linlicun fault (F7), Shilong fault (F8), Shaguoshu fault (F9), Lugu fault (F10), Yijiahaizi fault (F11), Yangfushan fault (F12), and Shejinuo fault (F13). The western fault includes the Shayema fault (F15), Dapingzi fault (F16), and Luji fault (F17). The plane structure of this section is complex with a high movement speed and strong activity. Historically, mainly strong earthquakes have occurred in this section, as the fault is of the stick slip activity mode (Tang et al. 2016). Mid-South section (II-3): from Lizhou to Xichang This area is approximately 15 km long and only includes the Hongshanzui fault (F14). The plane structure of the fault is simple with a high movement speed. Due to presence of the stick slip activity mode, many earthquake epicenters are distributed across this section. Two Ms 7.5 earthquakes occurred near the northern and southern ends of the F14 fault in the study area.
3. ***South section (III): the southern area of the city of Xichang***

   This section includes a slow-moving, low-activity fault. There are only minor, sporadic earthquakes, and the fault in this section largely belongs to the creep slip activity mode.

Large-scale landslide distribution along the Anninghe fault zone

Recent studies have revealed that more than 80% of landslides in the study area are distributed within 3 km of the Anninghe fault rupture zone (Zhou et al. 2021a, b). However, the existing research does not explain the piecewise difference in the distribution density of large-scale landslides along the Anninghe fault zone. According to the distribution characteristics of large-scale landslides in the study area, the corresponding relationship between the active section of the Anninghe fault zone and the distribution of large-scale landslides is analyzed.

Evolution characteristics and sliding mode of large-scale landslides

The evolution of a large-scale landslide is a complex geological process. The occurrence of a landslide is closely related to the geological conditions and human activity. In particular, the formation and evolution of a large-scale landslide are closely related to the spatial distribution of the regional active faults and the corresponding adjacent areas. Hovius and Meunier (2012) analyzed the relationship between the large-scale faults and the landslide evolution by using the examples of Wenchuan in Sichuan of China, Chi Chi in Taiwan, Niigata in Japan, Finisterre in Spain, and Northridge in the USA, and they pointed out that the mountain uplift caused by active faults was mainly balanced and coordinated by collapse, landslide, or denudation. Strong neotectonic movement has formed the landform of high mountains and valleys, with a large elevation difference and a strong potential energy, which easily lead to the formation of large-scale landslides (Fig. 7).

Remote sensing interpretation and geological surveys were conducted, and 57 large-scale landslides ($> 1.0 \times 10^6$ m^3) were found to be distributed within 20 km of both sides of the Anninghe fault zone, including 45 landslides ($1 \sim 10 \times 10^6$ m^3) and 12 landslides ($> 10 \times 10^6$ m^3) (Table 5). The investigation results show that 57 landslides are controlled by faults to varying degrees, and these landslides are called "fault-controlled landslides (FCLs)" in this paper. The main sliding modes of large-scale landslides controlled by the fault are summarized as follows.

1. ***Landslide-entirety fault-controlled type (LEFT): fault rock constituting the whole landslide body***

   As a large-scale regional fault zone, the width of the Anninghe fault fracture zone can reach hundreds of meters. A landslide can occur in the fault fracture zone, and the rock mass in the fault zone directly constitutes the sliding body due to favorable topographic conditions, such as those of the Zhaobishan landslide (Fig. 8a). The Mixiluogou fault (F5), with a 350 ~ 400 m wide fracture zone, passes through the middle of the failure slope. Continuous large-scale deformation and sliding have occurred in the fracture zone under rainfall conditions due to its poor stability.

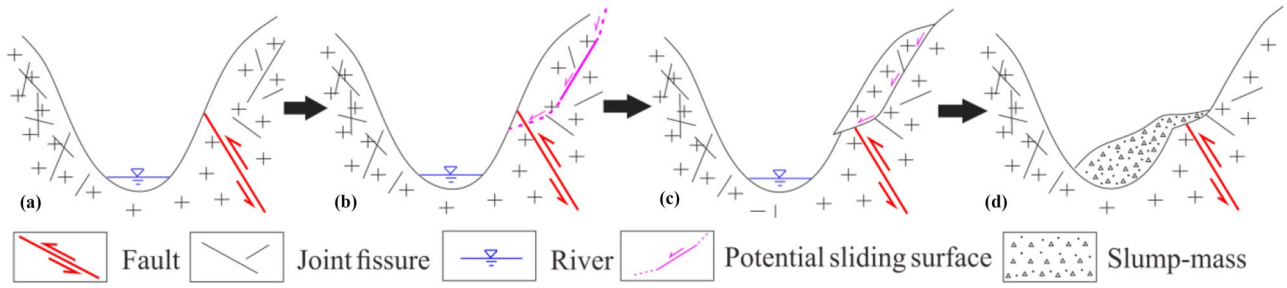

Fig. 7 Schematic change of fault–uplift–denudation (rockslide)

2. ***Landslide-toe fault-controlled type (LTFT): fault controlling the toe of a landslide***

In our field investigation, the authors found that faults passing through the foot of the slope play an important role in influencing the stability of the slope and the formation and evolution of landslides, especially the effect of superimposed earthquake. There are many destructive earthquakes along the Anninghe fault zone and its adjacent areas. Dabacha landslide, a typical example, was controlled by a fault passing through the toe of the slope and was triggered by a strong earthquake. The sliding direction runs from SW230° to EW270° and then to

Table 5 Characteristics of fault-controlled landslides in the Shimian to Xichang sections of the Anninghe fault zone

No	Name	Volume/10^4 m^3	Stability	Sliding mode	No	Name	Volume/10^4 m^3	Stability	Sliding mode
1	Waergou	150	Instable	LCFT	30	Manshuiwan	20,000	Stable	ELFT
2	Saikeniluo	150	Basically stable	LCFT	31	Datanghe 3#	150	Basically stable	LEFT
3	Waquyijia	100	Instable	LCFT	32	Datanghe 1#	100	Basically stable	LEFT
4	Dagangshan	120	Instable	LSFT	33	Mada	140	Basically stable	LCFT
5	Wachanggou	240	Basically stable	LCFT	34	Luonaige 3#	150	Instable	LCFT
6	Zhaobishan	455	Instable	LEFT	35	Gongyeyuan	1000	Basically stable	LCFT
7	Hunshuigou 1#	750	Basically stable	LEFT	36	Baitu	300	Stable	LSFT
8	Hunshuigou 2#	360	Instable	LEFT	37	Bainigou 1#	100	Instable	LEFT
9	Caogubaozi	150	Basically stable	ELFT	38	Bainigou 2#	100	Instable	LEFT
10	Daqiaoshuiku	100	Instable	LCFT	39	Chaowangpin	650	Stable	LCFT
11	Zhuanjinfang	300	Basically stable	LSFT	40	Kaili	112	Instable	LEFT
12	Dewu	500	Basically stable	LCFT	41	Juemo	8000	Stable	LCFT
13	Jiaodi	100	Basically stable	LCFT	42	Baozi	4500	Stable	LTFT
14	Luonaige 1#	400	Basically stable	LCFT	43	Datanghe 2#	250	Instable	LEFT
15	Luonaige 2#	160	Basically stable	LCFT	44	Donghe	678	Basically stable	LCFT
16	Dapin	3000	Stable	LTFT	45	Caishuzu	520	Basically stable	LCFT
17	Yanseitang	150	Instable	LTFT	46	Laobaozi	280	Stable	LCFT
18	Zhongba 1#	600	Basically stable	LEFT	47	Huishuigou	100	Instable	LEFT
19	Zhongba 2#	3500	Basically stable	LCFT	48	Yangcaigou	140	Instable	LSFT
20	Caishachang	500	Basically stable	LCFT	49	Zufu	1400	Instable	LCFT
21	Zhongba 5#	100	Basically stable	LEFT	50	Keluotou	300	Instable	LEFT
22	Dashuigou	750	Stable	LEFT	51	Manhagou	400	Stable	LCFT
23	Wangjiashan	1100	Stable	LCFT	52	Huipengzi	2000	Stable	LCFT
24	Fengjiapin	400	Stable	LSFT	53	Ganhaizi	100	Stable	LCFT
25	Heishahe 4#	500	Instable	LEFT	54	Meijian	4000	Stable	ELFT
26	Heishahe 3#	300	Instable	LEFT	55	Leiwu	2500	Stable	LCFT
27	Heishahe 2#	400	Instable	LEFT	56	Zuiwopin	2000	Stable	LCFT
28	Heishahe 1#	300	Basically stable	LEFT	57	Hebatou	100	Instable	LEFT
29	Dabaca	150	Stable	LTFT					

Sliding mode: *LEFT* landslide-entirety fault-controlled type, *LTFT* landslide-toe fault-controlled type, *LCFT* landslide-crown fault-controlled type, *LSFT* landslide-side fault-controlled type

NW310° due to the constraint of the downward terrain (Fig. 8b).

3. ***Landslide-crown fault-controlled type (LCFT): fault controlling the crown of a landslide***

   Compared to that of intact rock, the rock mass in this fault has poor mechanical strength. The mechanical strength of the fault, which passes through the middle and upper parts of the slope, can significantly influence and control the stability of the slope. The sliding-shearing deformation of the slope is controlled by the fault fracture zone. Then, large-scale failure occurs, leading to a landslide after continuous deformation (e.g., the Luonaige #1 landslide (Fig. 8c)). The slope has suffered multiple slides to the free face due to the Hongshanzui fault (F14), which passes through the crown of the landslide.

4. ***Landslide-side fault-controlled type (LSFT): fault controlling the lateral boundary of a landslide***

   Faults can not only control the crown of a landslide but can also control the lateral boundary of a landslide, which is the case of the Yangcaigou landslide. This landslide is controlled by a buried fault on the east side and is controlled by the Shawan fault (F6) on the west side (Fig. 8d). The Yangcaigou landslide is classified into three zones, i.e., landslides #1, #2, and #3. Landslide #1 is mainly located in the Shawan fault fracture zone and has developed between two faults.

Sectional characteristics of the density of large-scale landslides

Figure 9 shows that the Anninghe fault zone plays a prominent role in controlling the distribution of large-scale landslides. At farther distances to the Anninghe fault, the distribution density of large-scale landslides in the east–west direction is lower. However, the distribution density of large-scale landslides is uneven and can be divided into three sections in the north–south direction.

1. ***Low distribution quantity and density section***

   This section is approximately 70-km long and runs from Tianwan to Tuowu. There are 7 large-scale landslides, and only 2 landslides are within 3 km of the fault rupture zone. The distribution density of the landslides is 0.02 ~ 0.15 per 10 km^2, indicating that the influencing and controlling effects of the Anninghe fault are weak.

2. ***High distribution quantity and density section***

   This section is approximately 35-km long and runs from Tuowu to Mianning. There are a total of 20 large-

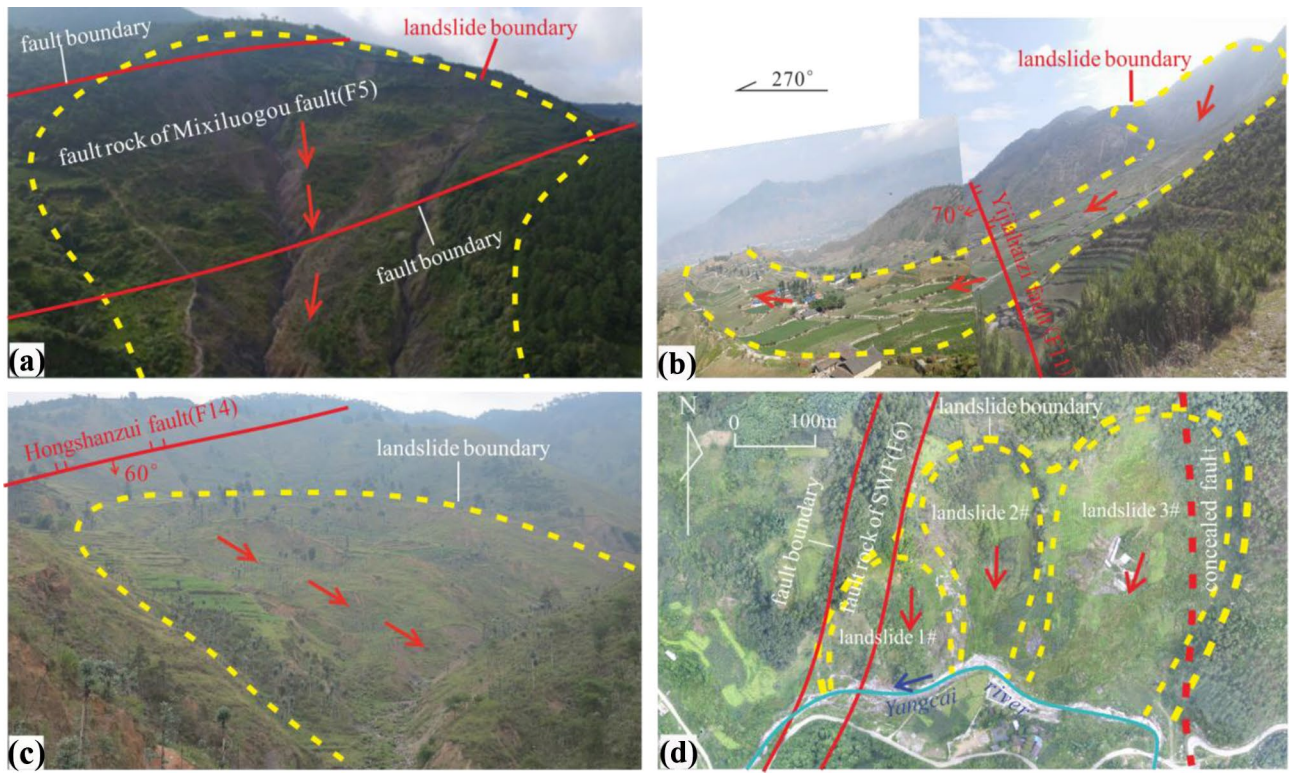

Fig. 8 Typical fault-controlled landslides, **a** LEFT (Zhaobishan landslide, No. 6); **b** LTFT (Dabaca landslide, No. 29); **c** LCFT (Luonaige landslide 1#, No. 14); **d** LSFT (Yangcaigou landslide, No. 48)

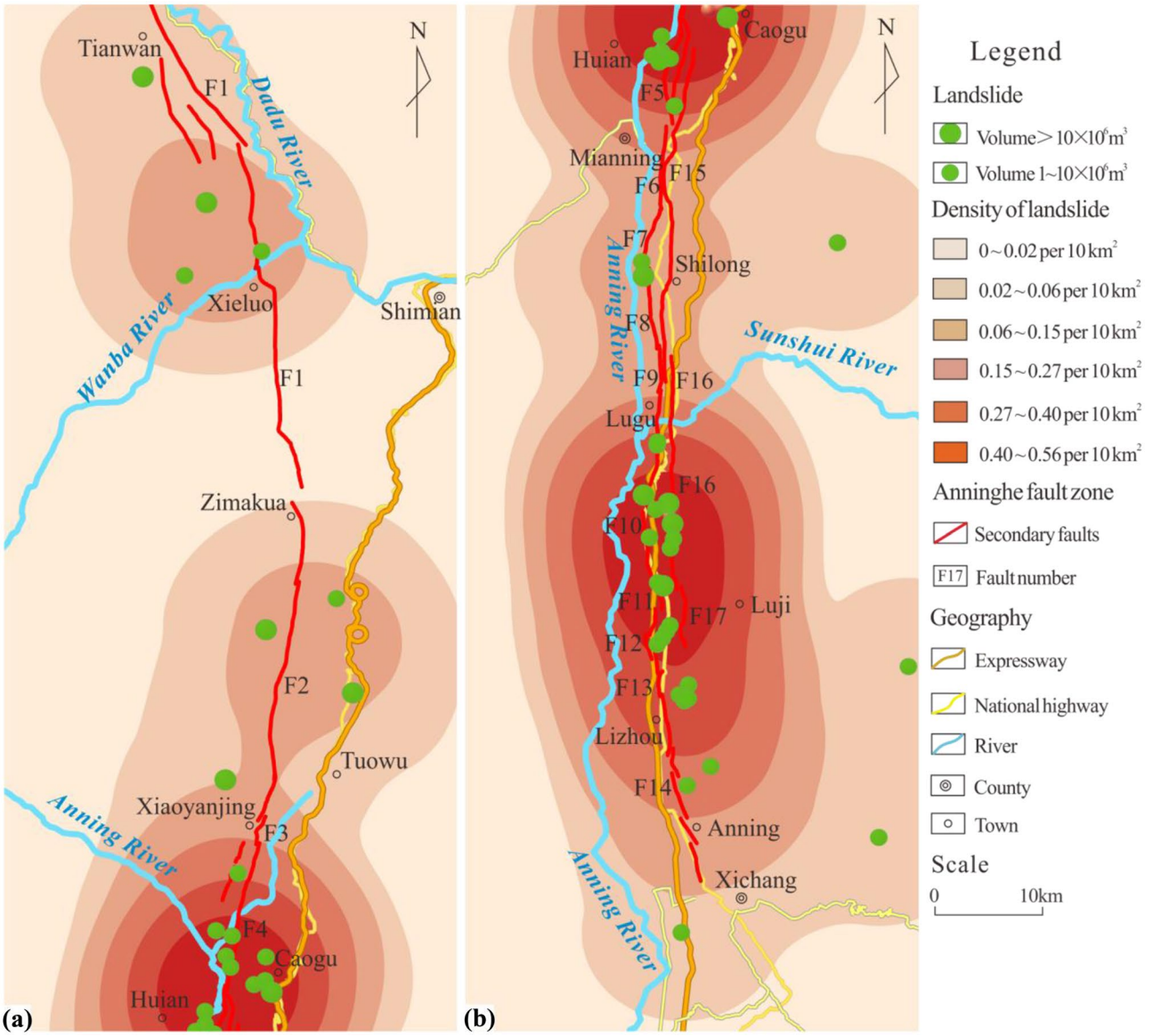

Fig. 9 Density diagram of fault-controlled landslides in the Tianwan to Xichang sections of the Anninghe fault zone: **a** Tianwan to Huian sections; **b** Huian to Xichang sections

scale landslides, and 19 are within 3 km of the fault rupture zone. Notably, the distribution density of large-scale landslides is 0.4 ~ 0.6 per 10 km^2 near Caogu and Huian, denoting the highest distribution density of large-scale fault-controlled landslides along the Anninghe fault zone.

3. ***Higher distribution quantity and density section***

   This section is approximately 70-km long and runs from Mianning to Xichang. There are 30 large-scale landslides, and 26 are within 3 km of the fault rupture zone. The length of the fault is only 30 km from the Lugu to Anning sections; however, there are 24 large-scale landslides near the fault rupture zone, and the distribution density of large-scale landslides is 0.3 ~ 0.6 per 10 km^2.

Relationship between large-scale landslides and the active section of the Anninghe fault zone

In general, the stronger present-day fault activity is, the higher the distribution density of landslides is according to the comprehensive analyses presented in Figs. 6 and 9, and Table 4. There is a good relationship between the sectional activity of the Anninghe fault zone and the distribution density of large-scale fault-controlled landslides. The Anninghe fault zone can be further divided into four sections based

on the present-day displacement rate, sliding mode, fault earthquake activity, and distribution density of large-scale landslides.

1. ***Section from Tianwan to Xiaoyanjing***
   The present-day displacement rate of the Anninghe fault is $1.2 \sim 1.66 \pm 1.66$ mm/a in this section with weak activity. The fault mainly belongs to the creep slip activity mode, and the stick slip activity mode is found in one section. Many earthquakes have occurred here over thousands of years; however, these earthquakes have been low or moderate in magnitude. The distribution density of large-scale landslides is less than 0.15 per 10 km^2.
2. ***Section from Xiaoyanjing to Mianning***
   The present-day displacement rate of the Anninghe fault zone is 2.98 ± 1.73 mm/a in this section with stronger activity. The fault belongs to the stick slip activity mode. Many earthquakes of moderate and large magnitudes have occurred in this section. The distribution density of landslides is $0.3 \sim 0.6$ per 10 km^2 in this section.
3. ***Section from Mianning to Lugu***
   Similar to that of the section from Xiaoyanjing to Mianning, the present-day displacement rate is 2.98 ± 1.73 mm/a in this section with stronger activity. The fault mainly belongs to the stick slip activity mode. Most earthquakes have been of moderate magnitude in this section. The distribution density of landslides is $0.1 \sim 0.3$ per 10 km^2 in this section.
4. ***Section from Lugu to Xichang***
   The present-day displacement rate of the Anninghe fault zone is 8.15 ± 1.31 mm/a in this section with strong activity. The fault belongs to the stick slip activity mode. There have been many earthquakes of high magnitude in this section. Due to the numerous large-scale landslides that have developed in this section, the distribution density of landslides is $0.3 \sim 0.6$ per 10 km^2.

Discussion

From engineering geological investigations of the Anninghe fault zone, Zhou et al. (2021a, b) found large-scale landslides distributed in a belt along the fault zone. In addition, the distribution density of large-scale landslides is closely related to the sectional activity of the fault zone. Therefore, the relationship between the present-day sectional activity of the Anninghe fault zone and the distribution density of large-scale fault-controlled landslides was analyzed using a variety of technical methods. The results show that the stronger the present-day activity of a fault is, the larger the distribution density of large-scale landslides is. There is thus a positive correlation between present-day fault activity and fault-controlled landslide distribution density along the Anninghe fault zone.

There are two main causes of this phenomenon. During the slow creep of a fault with strong activity, gaps and tensile cracks form in the slope that the fault passes through. This phenomenon can result in the subsidence deformation or local stress concentration of the slope rock mass, causing or aggravating landslide disasters (Zhang et al. 2015, 2017). In addition, a rock mass around a fault often causes extrusion or tension deformation and failure due to the creep deformation of the fault. This phenomenon can result in tension cracks and the disintegration of the slope rock mass, inducing landslide disasters and reducing the stability of a rock mass slope (Yao et al. 2017). Such a fault exhibits a very low creep deformation speed or almost no creep deformation; however, the degree of tensile deformation or stress concentration of the slope rock mass around the fault is low. There are relatively few landslides along a fault with weak activity or no activity, and they are mainly found the sliding control boundaries of large-scale landslides.

The stronger the activity of a fault zone is, the higher the frequency and magnitude of an earthquake will be. There are more large-scale landslides closer to epicenters and under greater earthquake intensity (Tolga et al. 2011). Compared to those caused by faults with weak activity, more landslides are triggered by major faults with strong activity.

It should be noted that there is no absolute positive quantitative correlation between the present-day displacement rate of a fault and the distribution density of large-scale fault-controlled landslides near the Anninghe fault zone. The distribution density of large-scale landslides is significantly different, with almost 2 times the value found in the Xiaoyanjing to Mianning sections and Mianning to Lugu sections of the Anninghe fault; however, the present-day displacement rate of the fault is the same based on GPS measurement results. This is the case because the number and scale of landslides are related to the spatial location, the active characteristics of faults, rainfall, and human engineering activities. These values are also related to the accuracy of geological surveys and the density of GPS monitoring stations.

In addition, only landslides of more than 1 million m^3 were considered in this study, and landslides of less than 1 million m^3 were not included in the statistical analysis. This variable may also impact the quantitative value of the distribution density of fault-controlled landslides. However, it should not significantly influence the results of our long-term investigation and substantial work. Recently, some new GPS monitoring stations have been established. We will continue to carry out remote sensing image interpretation and geological surveys to illustrate the relationship between the distribution characteristics of small- and medium-scale

landslides and the present-day sectional activity of the Anninghe fault zone.

The occurrence of a landslide is related to many factors, such as landform, lithology, rock mass structure, active fault, rainfall, human activity, and earthquake. Through the 5-year engineering geological survey, however, we found that most landslides locate at the Anninghe active fault zone and its adjacent areas (Zhou et al. 2021a, b). Statistical results show that more than 80% of large-scale landslides were within 2–3 km of the Anninghe fault rupture zone. The distribution of these large-scale landslides has an aggregation effect. The density of landslides per million square meter is positively related to the fault activity along the north–south direction. It should be noted that the 57 landslides in Table 5 refer to the large-scale fault-controlled landslides controlled by the Anninghe active fault. The small-scale landslides caused by rainfall and human activities are excluded in this paper.

Conclusions

The Anninghe fault zone is an important regional boundary fault at the eastern margin of the Tibetan Plateau. According to geological survey results, the Anninghe fault zone is further divided into 17 Holocene secondary faults. By spatial geometric shape, structure, activity mode, intensity, and seismic activity, the Anninghe fault can be divided into three sections, i.e., northern, middle, and southern sections. The northern section runs from Tianwan to Zimakua, its activity and displacement rate are moderate, and its structure is moderately complex. The earthquakes that have occurred in this section are mainly low- and moderate-magnitude earthquakes occurring due to the creep slip activity mode of the fault. The southern section is located in the southern area of the city of Xichang and is characterized by weak activity and a low displacement rate. Only sporadic, small earthquakes have occurred here, and the fault belongs to the creep slip activity mode. The middle section runs from Zimakua to Xichang and has a complex fault structure and strong activity. Destructive earthquakes have mainly occurred in this section, the displacement rate is high, and the fault belongs to the stick slip activity mode. The middle section can be further divided into three subsections, i.e., Zimakua to Xiaoyanjing, Xiaoyanjing to Lizhou, and Lizhou to Xichang. Generally, the activity of the middle section is the strongest, followed by that of the northern section and then that of the southern section.

Four sliding modes of large-scale landslides controlled by the Anninghe fault zone are summarized, i.e., the landslide-entirety fault-controlled type (LEFT), landslide-crown fault-controlled type (LCFT), landslide-side fault-controlled type (LSFT), and landslide-toe fault-controlled type (LTFT). In relation to typical landslides, the characteristics and mechanisms of the four sliding modes were analyzed and expounded.

The activity of the Anninghe fault shows a positive correlation with the number and density of large-scale fault-controlled landslides. The present-day displacement rate is $1.2 \sim 1.66 \pm 0.66$ mm/a in the section from Tianwan to Xiaoyanjing, and the distribution density of large-scale landslides is less than 0.15 per 10 km^2 in this low-activity area. The present-day displacement rate is 2.98 ± 2 mm/a in the sections from Xiaoyanjing to Mianning and Mianning to Lugu, and the distribution densities of large-scale landslides in the area with stronger activity are $0.3 \sim 0.6$ per 10 km^2 and $0.1 \sim 0.3$ per 10 km^2, respectively. The present-day displacement rate is 8.15 ± 8 mm/a in the section from Lugu to Xichang, and the distribution density of large-scale landslides in the area with strong activity is $0.3 \sim 0.6$ per 10 km^2.

Funding This research was supported by the China Geological Survey Projects (no. 20160272, 20211379), the Second Tibetan Plateau Scientific Expedition and Research Program (no. 2019QZKK0904), and Sichuan Science and the Technology Program of China (no. 2020YFS0296).

Declarations

Competing interests The authors declare no competing interests.

References

Ahmad R (2021) Geometric and kinematic characteristics of the Khazar and North Alborz Faults: links to the structural evolution of the North Alborz-South Caspian boundary, Northern Ira. J Asian Earth Sci 213:104755. https://doi.org/10.1016/j.jseaes.2021.104755

Chen ZQ, He C, Yang WB, Guo WQ, Li Z, Xu GW (2020) Impacts of geological conditions on instability causes and mechanical behavior of large-scale tunnels: a case study from the Sichuan-Tibet highway, China. Bull Eng Geol Env 79:3667–3688. https://doi.org/10.1007/s10064-020-01796-w

Cheng J, Xu XW, Yao Q, Yang XD, Chen H (2021) Seismic hazard of multi-segment rupturing for the Anninghe–Zemuhe–Daliangshan fault region, southeastern Tibetan Plateau: constraints from geological and geodetic slip rates. Nat Hazards. https://doi.org/10.1007/s11069-021-04643-7

He HL, Ikeda Y (2007) Faulting on the Anninghe fault zone, Southwest China in Late Quaternary and its movement model. Acta Seismol Sin 20:571–583. https://doi.org/10.1007/s11589-007-0571-4

He HL, Oguchi T (2008) Late Quaternary activity of the Zemuhe and Xiaojiang faults in southwest China from geomorphological mapping. Geomorphology 96:62–85. https://doi.org/10.1016/j.geomorph.2007.07.009

Ho GR, Chang PY, Lee JC, Jonathan CL, Chen PT, Hsu HL (2020) Surface traces and related deformation structures of the southern Sanyi Fault, Taiwan, as deduced from field mapping, electrical- resistivity tomography, and shallow drilling. Eng Geol 273:105690. https://doi.org/10.1016/j.enggeo.2020.105690

Hovius N, Meunier P (2012) Earthquake ground motion and patterns of seismically induced landsliding. Landslide. https://doi.org/10.1017/CBO9780511740367.004

Kanaori Y, Miyakoshi K, Kakuta T, Satake Y (1980) Dating fault activity by surface textures of quartz grains from fault gouges. Eng Geol 16:243–262. https://doi.org/10.1016/0013-7952(80)90018-6

Kanaori Y, Tanaka K, Miyakoshi K (1985) Further studies on the use of quartz grains from fault gouges to establish the age of faulting. Eng Geol 21:175–194. https://doi.org/10.1016/0013-7952(85)90004-3

Li AM, Takao M, Wan TF (1998) Tectonic characteristics of the central segment of the Tancheng-Lujiang fault zone, Shandong Peninsula, eastern China. Tectonophysics 293:85–104. https://doi.org/10.1016/S0040-1951(98)00087-0

Osmundsen PT, Henderson I, Lauknes TR, Larsen Y, Redfield TF, Dehls J (2009) Active normal fault control on landscape and rock-slope failure in northern Norway. Geology 37(2):135–138. https://doi.org/10.1130/G25208A.1

Qu W, Lu Z, Zhang Q, Hao M, Wang QL, Qu FF, Zhu W (2018) Present-day crustal deformation characteristics of the southeastern Tibetan Plateau and surrounding areas by using GPS analysis. J Asian Earth Sci 163:22–31. https://doi.org/10.1016/j.jseaes.2018.05.021

Ran YK, Chen LC, Cheng JW, Gong HL (2008) Late Quaternary surface deformation and rupture behavior of strong earthquake on the segment north of Mianning of the Anninghe fault. Sci China, Ser D-Earth Sci 51:1224–1237. https://doi.org/10.1007/s11430-008-0104-6

Ren ZK (2014) Late Quaternary deformation features along the Anninghe Fault on the eastern margin of the Tibetan Plateau. J Asian Earth Sci 85:53–65. https://doi.org/10.1016/j.jseaes.2014.01.025

Ren ZK, Lin AM, Rao G (2010) Late Pleistocene-Holocene activity of the Zemuhe Fault on the southeastern margin of the Tibetan Plateau. Tectonophysics 495:324–336. https://doi.org/10.1016/j.tecto.2010.09.039

Scheingross JS, Minchew BM, Mackey BH, Simons M, Lamb MP, Hensley S (2013) Fault-zone controls on the spatial distribution of slow-moving landslides. Geol Soc Am Bull 125(3–4):473–489. https://doi.org/10.1130/B30719.1

Stead D, Wolter A (2015) A critical review of rock slope failure mechanisms: The importance of structural geology. J Struct Geol 74:1–23. https://doi.org/10.1016/j.jsg.2015.02.002

Tang WQ, Zhang YS, Zhang QZ, Zhou HF, Pan ZX, Li J, Yang C (2016) Present-day block movement and fault activity on the eastern margin of the Tibet Plateau. Acta Geologica Sinica (English Edition) 90:456–466. https://doi.org/10.1111/1755-6724.12683

Tolga G, Fan XM, Cees JW, Huang RQ, Xu Q, Tang C, Wang GH (2011) Distribution pattern of earthquake-induced landslides triggered by the 12 May 2008 Wenchuan earthquake. Geomorphology 133:152–167. https://doi.org/10.1016/j.geomorph.2010.12.030

Vick LM, Bhme M, Rouyet L, Bergh SG, Lauknes TR (2020) Structurally controlled rock slope deformation in northern Norway. Landslides 17:1745–1776. https://doi.org/10.1007/s10346-020-01421-7

Wang H, Ran YK, Chen LC, Li YB (2017) Paleoearthquakes on the Anninghe and Zemuhe fault along the southeastern margin of the Tibetan Plateau and implications for fault rupture behavior at fault bends on strike-slip faults. Tectonophysics 721:167–178. https://doi.org/10.1016/j.tecto.2017.08.030

Wang H, Ran YK, Li YB, Gomez F, Chen LC (2014) A 3400-year-long paleoseismologic record of earthquakes on the southern segment of Anninghe fault on the southeastern margin of the Tibetan Plateau. Tectonophysics 628:206–217. https://doi.org/10.1016/j.tecto.2014.04.040

Wang YZ, Wang EN, Shen ZK, Wang M, Gan WJ, Qiao XJ, Meng GJ, Li TM, Tao W, Yang YL, Cheng J, Li P (2008) GPS-constrained inversion of present-day slip rates along major faults of the Sichuan-Yunnan region, China. Sci China Ser D Earth Sci 51(9):1267–1283. https://doi.org/10.1007/s11430-008-0106-4

Wen XZ, Ma SL, Xu XW, He YN (2008) Historical pattern and behavior of earthquake ruptures along the eastern boundary of the Sichuan-Yunnan faulted-block, southwestern China. Phys Earth Planet Inter 168:16–36. https://doi.org/10.1016/j.pepi.2008.04.013

Wu RA, Zhang YS, Guo CB, Yang ZH, Tang J, Su FR (2020) Landslide susceptibility assessment in mountainous area: a case study of Sichuan-Tibet railway, China. Environ Earth Sci 79:157–173. https://doi.org/10.1007/s12665-020-8878-8

Xu YB (1988) Study on the combinations of the SEM characteristics of the mineral arrangements of the gouges and the patterns of the movements of Anninghe active fault zone. N Seismol J 10(3):39–44. (in Chinese)

Xu YB, Tang RC, Zhang TG (1987) The quantitative analysis for the characteristic of SEM micro-surface textures on quartz fragments of Aninghe fault zone and the estimation about the active state of the fault zone. Earthq Res China 3(3):68–74. (in Chinese)

Xu YR, Zeng JL, Mark BA, Zhang WH, Du P (2020) Landslides of the 1920 Haiyuan earthquake, northern China. Landslides 18:935–953. https://doi.org/10.1007/s10346-020-01512-5

Yang Y, Li Y, Guan ZJ, Chen Z, Zhang L, Lv CJ, Sun FX (2018) Correlations between the radon concentrations in soil gas and the activity of the Anninghe and the Zemuhe faults in Sichuan, southwestern of China. Appl Geochem 89:23–33. https://doi.org/10.1016/j.apgeochem.2017.11.006

Yao X, Li LJ, Zhang YS, Zhou ZK, Liu XH (2017) Types and characteristics of slow-moving slope geohazards recognized by TS-InSAR along Xianshuihe active fault in the eastern Tibet Plateau. Nat Hazards 88:1727–1740. https://doi.org/10.1007/s11069-017-2943-y

Ye F, Fu WX, Zhou HF, Liu Y, Ba RJ, Zheng S (2021) The "8·21" rainfall-induced Zhonghaicun landslide in Hanyuan County of China: surface features and genetic mechanisms. Landslides 18:3421–3434. https://doi.org/10.1007/s10346-021-01722-5

Yi GX, Wen XZ, Fan J, Wang SW (2004) Assessing current faulting behaviors and seismic risk of the Anninghe-Zemuhe fault zone from seismicity parameters. Acta Seismol Sin 17:322–333. https://doi.org/10.1007/s11589-004-0054-9

Zhang BL, Lin CY, Fang ZJ, Liu GF (1994) Microstructural features of fault gouges in active fault and their implication. Chin Sci Bull 39(4):312–317

Zhang BL, Lin CY, Shi LB (2002) Microstructural features of fault gouges from Tianjing-shan-Xiangshan fault zone and their geological implications. Sci China Ser D Earth Sci 45:72–80. https://doi.org/10.1007/bf02879698

Zhang YS, Guo CB, Lan HX, Zhou NJ, Yao X (2015) Reactivation mechanism of ancient giant landslides in the tectonically active zone: a case study in Southwest China. Environ Earth Sci 74:1719–1729. https://doi.org/10.1007/s12665-015-4180-6

Zhang YS, Yang ZH, Guo CB, Wang T, Wang DH, Du GL (2017) Predicting landslide scenes under potential earthquake scenarios in the Xianshuihe fault zone, Southwest China. J Mt Sci 14:1262–1278. https://doi.org/10.1007/s11629-017-4363-6

Zhao B, Wang YS, Wu JF, Su LJ, Liu JW, Jin G (2021) The Mogangling giant landslide triggered by the 1786 Moxi Ms 7.75 earthquake, China. Nat Hazards 106:459–485. https://doi.org/10.1007/s11069-020-04471-1

Zhou HF, Fu WX, Ye F, Chen ZF (2021a) Study on sliding-shearing deformation and failure mode of rock slope with steep weak structural plane. Earth Sci 46(4):1437–1446. https://doi.org/10.3799/dqkx.2020.097. (in Chinese)

Zhou HF, Liu B, Ye F, Fu WX, Tang WQ, Qin YD, Fang T (2021b) Landslide distribution and sliding mode control along the Anninghe fault zone at the eastern edge of the Tibetan Plateau. J Mt Sci 18(8):2094–2107. https://doi.org/10.1007/s11629-020-6573-6